Progress In Electromagnetics Research C, Vol. 74, 51–61, 2017

Compact Microstrip Lowpass Filter with an Ultra-Wide Stopband and Sharp Transition Band Using T-Shaped and Polygon Resonators

Arash Abdipour and Ashkan Abdipour*

Abstract—In this paper, a lowpass filter with −3 dB cutoff frequency of 5.3 GHz using T-shaped and polygon resonators is presented. The applied resonators create a sharp transition band of 0.2 GHz from −3 dB to −40 dB. To obtain an ultra-wide stopband about 54 GHz ($10.18 f_c$) with a suppressing level of −21 dB, two different suppressing cells are employed. The overall circuit size is 59.16 mm^2, which indicates a small occupied area. To clarify the performance of each resonator and describe the location of the transition zeros, exact equations based on the equivalent LC circuits have been calculated.

1. INTRODUCTION

The need of omitting spurious frequencies in order to increase the quality of sending and receiving signals leads to designing lowpass filters with good in-band and out-band performances. These items have been studied and improved by utilizing several methods. For example, stepped impedance hairpin resonator with radial stubs has been utilized to design a LPF with wide stopband, in [1]. Unfortunately, this circuit has not been able to provide a sharp transition band. To design a LPF with wide stopband a cascaded microstrip coupled-line hairpin unit, semi-circle defected ground structures (DGSs) and semi-circle stepped-impedance shunt stubs have been used [2]. However, employing the DGS in the LPFs makes it incapable of being used on metal surfaces. In [3], a LPF with an ultra-wide stopband employing LC resonant structures and transformed radial stubs is proposed. However, the circuit size is relatively large. A microstrip lowpass filter featuring compact size and ultra-wide stopband by utilizing both triangular and polygonal patch resonators is designed [4]. In [5], to design a LPF with an ultra- wide stopband triangular and radial patch resonators have been employed. However, the proposed circuits in [4] and [5] suffer from a gradual transition band and a low level of suppression. In addition to the mentioned challenges, gradual transition band and low level of relative stopband bandwidth [6–8], a narrow stopband region [9], occupying a large circuit size [10] have affected the frequency response of each case, negatively. Another method to design a LPF is using asymmetric high-low impedance patches, which has been reported in [11], but this structure does not have a good in-band performance. In this article, a compact lowpass filter with −3 dB cut-off frequency of 5.3 GHz has been proposed. In the designed LPF, by combining T-shaped resonators, polygon patches and two different suppressing cells a sharp roll-off and an ultra-wide stopband have been obtained. In addition, the locations of transmission zeros of the main resonators on the basis of their equivalent LC circuits have been calculated, separately. Despite the above-mentioned challenges, the trial to achieve more applicable designs with various structures is undeniable [13–16].

Received 19 December 2016, Accepted 31 March 2017, Scheduled 15 May 2017
* Corresponding author: Ashkan Abdipour (Ashkan_Abdipour@yahoo.com).
The authors are with the Young Researchers and Elite Club, Kermanshah Branch, Islamic Azad University, Kermanshah, Iran.

2. LOWPASS FILTER DESIGN

This section introduces the employed resonators and explains the procedure of designing, step by step. The configuration and equivalent LC circuit of T-shaped resonator have been illustrated in Figures 1(a) and (b). As it is illustrated in Figure 1(b), L_{1T} is the equivalent inductor caused by the main transmission line determined by T1. The designed T-shaped resonators are modeled by L_{2T} and C_{2T}, where L_{2T} determines high impedance transmission lines of this resonator (T3), and C_{2T} shows open-circuit transmission line (T2).

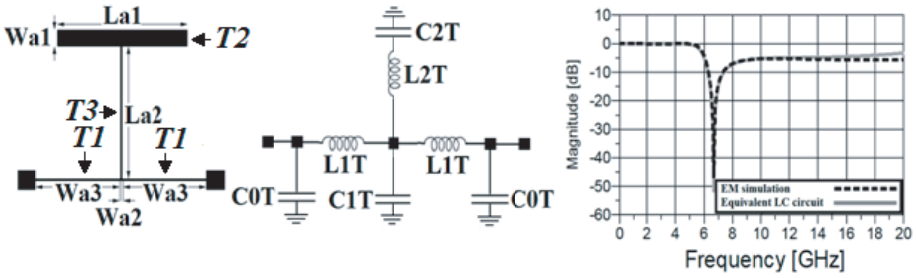

Figure 1. (a) The configuration of the T-shaped resonator. (b) The equivalent LC circuit of the T-shaped resonator. (c) The EM simulation result and frequency response of LC circuit of the T-shaped resonator.

Furthermore, C_{0T} and C_{1T} present the capacitance between the microstrip structure and the ground. The values of inductors and capacitors of the shown LC circuit in Figure 1(b) are: $L_{1T} = 0.9\,\text{nH}$, $L_{2T} = 2\,\text{nH}$, $C_{0T} = 16.5\,\text{fF}$, $C_{1T} = 98.4\,\text{fF}$, $C_{2T} = 285\,\text{fF}$. The EM simulation result and frequency response of LC circuit of the T-shaped resonator have been shown in Figure 1(c). According to the simulation results, the proposed resonator has a $-3\,\text{dB}$ operating frequency of $5.573\,\text{GHz}$. In the whole passband region, the insertion loss is close to zero. Moreover, the designed resonator has a transmission zero at $6.832\,\text{GHz}$ with corresponding attenuation level of $-51.13\,\text{dB}$ leading to having a desired transition band. Obviously, transition zeros affect the cut-off frequency, the slop of the transition band and also the wideness of the stopband. Moreover, finding transition zeros according to the equivalent LC circuits can clarify the effect of each section of the resonators on the frequency response and the importance of them. Thus, to calculate transition zeros of the T-shaped resonators, the transfer functions based on equivalent LC circuit will be extracted. Transfer function and transition zero of the this resonator are given by Eqs. (1) and (2), respectively, as follows:

$$\frac{V_{out-T}}{V_{in-T}} = \frac{R + (RL_{2T}C_{2T})S^2}{R + (2L_{1T})S + AS^2 + BS^3 + CS^4 + DS^5 + ES^6} \tag{1}$$

where

$$\begin{aligned}
A &= (RL_{1T}C_{1T} + RL_{1T}C_{2T} + 2RL_{1T}C_{0T} + RL_{2T}C_{2T}).\\
B &= (L_{1T}^2C_{1T} + L_{1T}^2C_{2T} + 2L_{1T}L_{2T}C_{2T}).\\
C &= (RL_{1T}L_{2T}C_{0T}C_{2T} + RL_{1T}L_{2T}C_{1T}C_{2T} + RL_{1T}^2C_{0T}C_{1T} + RL_{1T}^2C_{0T}C_{2T}).\\
D &= (RL_{1T}^2L_{2T}C_{1T}C_{2T}).\\
E &= (RL_{1T}^2L_{2T}C_{0T}C_{1T}C_{2T}).
\end{aligned}$$

$$f_{z-T} = \frac{1}{2\pi}\sqrt{\frac{1}{L_{2T}C_{2T}}} \tag{2}$$

Note that (R) in transfer functions refers to the resistance of matching. As can be seen in Equation (2), the location of transmission zero can be adjusted by changing the capacitances and inductances values. For instance, according to Equation (2), L_{2T} and C_{2T} affect the transition zero of the T-shaped resonator, significantly. To clarify the effects of changing L_{2T} and C_{2T} on the frequency response, their

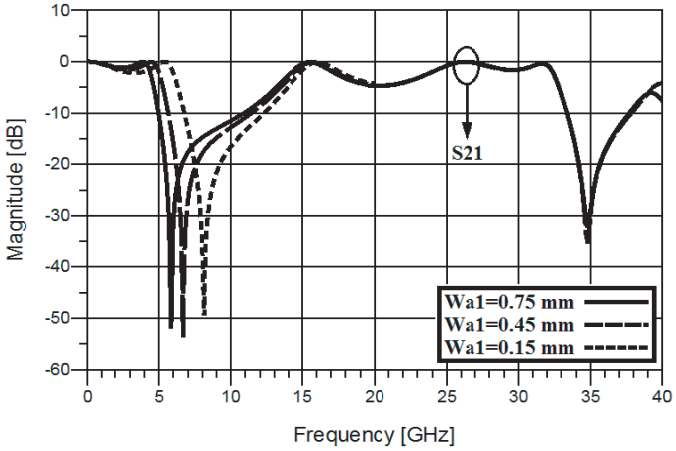

Figure 2. The behavior of the proposed primary resonator against changing the value of W_{a1}.

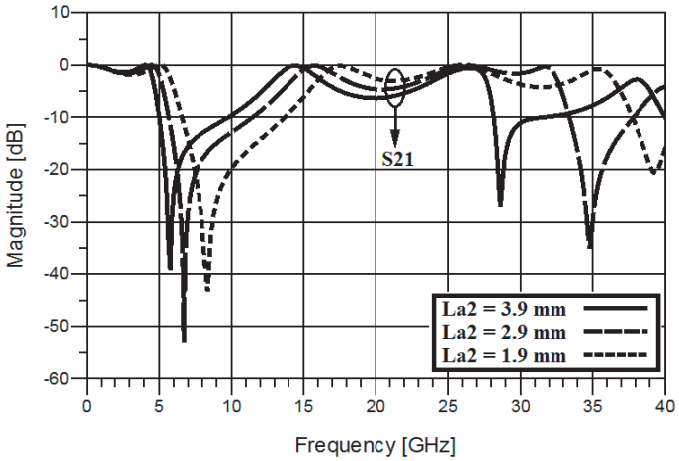

Figure 3. The behavior of the proposed primary resonator against changing the value of L_{a2}.

corresponding microstrip realizations can be considered instead. Thus, several full-wave simulations versus W_{a1} and L_{a2} have been plotted in Figures 2 and 3, respectively. Figure 2 shows the behavior of the mentioned T-shaped resonator against changing the value of W_{a1}. By increasing the value of W_{a1} from 0.15 to 0.75 mm with steps of 0.3, the transition zero at 8.33 GHz will move to lower frequencies causing a sharper transition band. Note that, this behavior had been predicted by Equation (2). The frequency response of the T-shaped resonator against changing L_{a2} has been shown in Figure 3. As it is observed, by increasing the value of L_{a2} the transition zeros will approach to lower frequencies, as it was anticipated by Equation (2). This leads to a sharper skirt performance. It is observed that changing the values of W_{a1} and L_{a2} has affected the operating frequency.

The configuration of the polygon resonator and its equivalent LC circuit has been shown in Figures 4(a) and (b), respectively. The dimensions of the shown polygon resonator in Figure 4(a) are: $W_{b1} = 0.3$, $W_{b2} = 0.1$, $L_{b0} = 2.1$, $L_{b1} = 3.7$, $L_{b2} = 2.5$, $L_{b3} = 1.8$, $L_{b5} = 3.9$, $L_{b6} = 0.7$, $L_{b7} = 1$, $L_{b8} = 1.1$ (all in millimeter).

The values of inductors and capacitors of the illustrated LC circuit in Figure 4(b) are: $L_{0p} = 1.116$ nH, $L_{1p} = 0.65$ nH, $L_{2p} = 1.904$ nH, $C_{1p} = 12.5$ pF, $C_{2p} = 160$ pF, $C_{3p} = 420$ fF, $C_{gp} = 21.7$ fF. In Figure 4(b), the designed polygon patches and the gap determined by W_{b1} are modeled by C_{3p} and C_{gp}, respectively. Moreover, L_{0p}, L_{2p} and L_{1p} account for the high impedance transmission lines which are shown by L_{b4}, L_{b5} and L_{b6}. Furthermore, C_{1p} and C_{2p} present the capacitance between the microstrip structure and the ground. As it is observed from the simulation results depicted in Figure 4(c), the cut-

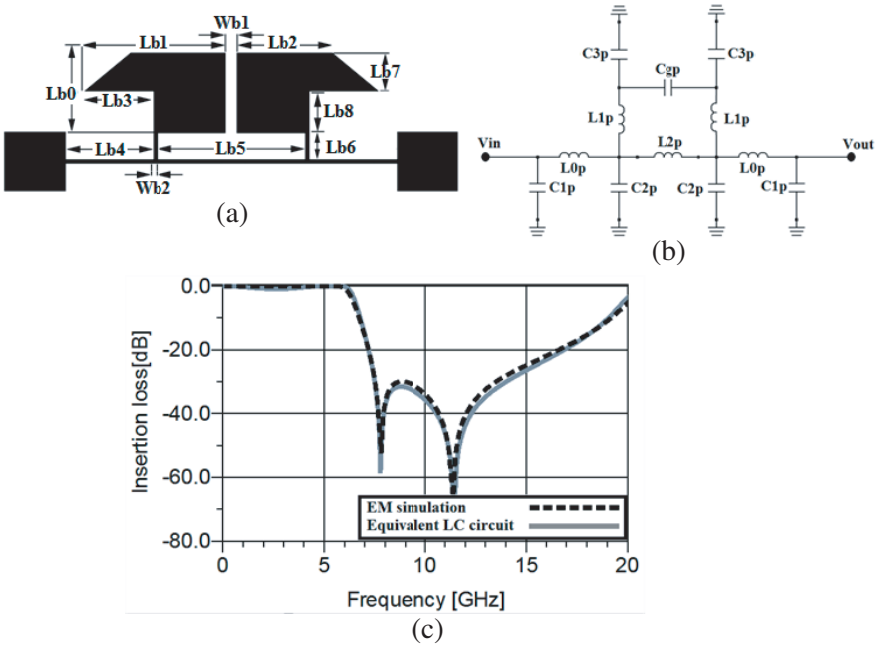

Figure 4. (a) The configuration of the polygon resonator. (b) The equivalent LC circuit of the polygon resonator. (c) The EM simulation result and frequency response of LC circuit of the polygon resonator.

off frequency of the presented resonator with polygon patches is located on 6.435 GHz. The stopband of this resonator suppress spurious frequencies from 6.89 GHz to 17.38 GHz with corresponding attenuation level of -20 dB. The insertion loss is approximately 0.093 dB from DC to 5.87 GHz and indicates an acceptable response in the passband. Moreover, the designed resonator creates two transmission zeros at 8.23 GHz and 11.56 GHz with corresponding attenuation levels of -58.13 dB and 72.33 dB, respectively, leading to a desired rejection band. To explain which lump elements of LC circuit and consequently which corresponding microstrip lines determine the location of the transmission zeros, the transfer function of the lumped circuit has been extracted. Transfer function and transition zeros of this structure can be given as follows ($\alpha = L_{0p}, b = L_{1p}, d = L_{2p}, g = C_{gp}, w = C_{3p}, c = C_{2p}$):

$$\frac{V_{out}}{V_{in}} = \frac{(Rb + A's^2 + B's^4)}{\alpha s[(C' + D')s^8 + (E' + F')s^6 + (H' + I')s^4 + (L' + M')s^2 + (3 + 3R)]} \tag{3}$$

where

$$\begin{aligned}
A' &= bR(dg + 2bg + 2bw).\\
B' &= Rb^3w(2g + w).\\
C' &= b^3wd(2gc^2 + c^2 + 4cw + 8cg + 2gc^2R).\\
D' &= b^3d + w^2c^2R.\\
E' &= b^2wc(4gb + 2cwd + 2bcw + 4dg + 2dw + 8d).\\
F' &= b^2(8cgd + 8bgw + 8wdg + 4w^2b + 4w^2d + 2Rcgdw + Rcw^2d).\\
H' &= db(6cRw + Rc^2 + 4Rgw + 2Rw^2 + 6Rcg + 4cw + c^2 + w^2 + 4gc + 8w + 8g).\\
I' &= b^2(4Rcw + 6Rgw + 3Rw^2 + 4Rcg + 8w + 2gw + w^2 + 8g).\\
L' &= dR(3c + 3w + 3g).\\
M' &= b(2Rc + 6Rw + 6Rg + 4 + 2c + 6w + 6g + 4gwb + 4bcg + 2bw^2 + 4bwc).
\end{aligned}$$

$$f_{z1-p} = \frac{1}{2\sqrt{2}\pi}\sqrt{\frac{F + \sqrt{G \cdot C_{gp}}}{H}} \tag{4}$$

where

$$F = 2L_{1p}C_{gp} + L_{2p}C_{gp} + 2L_{1p}C_{3p}.$$
$$G = 4L_{1p}^2C_{gp} + 4L_{1p}L_{2p}C_{gp} + L_{2p}^2C_{gp} + 4L_{1p}L_{2p}C_{3p}.$$
$$H = 2L_{1p}^2C_{gp}C_{3p} + L_{1p}^2C_{3p}^2.$$

$$f_{z2-p} = \frac{1}{2\sqrt{2}\pi}\sqrt{\frac{I - \sqrt{J \cdot C_{gp}}}{K}} \tag{5}$$

where

$$I = 2L_{1p}C_{gp} + L_{2p}C_{gp} + 2L_{1p}C_{3p}.$$
$$J = 4L_{1p}^2C_{gp} + 4L_{1p}L_{2p}C_{gp} + L_{2p}^2C_{gp} + 4L_{1p}L_{2p}C_{3p}.$$
$$K = 2L_{1p}^2C_{gp}C_{3p} + L_{1p}^2C_{3p}^2.$$

Similarly, the effects of the values of the inductors and capacitors affecting the frequency response will be studied based on the corresponding microstrip realizations. Clearly, the values of L_{1p}, L_{2p}, C_{gp} and C_{3p} can be used to control the location of transition zeros of the polygon resonator, effectively. Thus, to find their effects on the frequency response of the shown resonator in Figure 4(a), the dimensions of their corresponding microstrip realizations have been changed. Figures 5 and 6 plot several full-wave simulations versus L_{b0} and L_{b6}, respectively. Figure 5 illustrates the behavior of the polygon resonator against changing the value of L_{b0}. By increasing the value of L_{b0} from 1.65 to 2.55 mm with steps of 0.45, the transition zero at 8.981 GHz will move to lower frequencies causing a sharper transition band. The frequency response of this resonator against changing L_{b6} is indicated in Figure 6.

Clearly, by increasing the value of L_{b6} from 0.2 to 1.2 mm with steps of 0.5, the transition zeros will be close to lower frequencies. This leads to a sharper skirt performance. As can be observed, by increasing the values of both variables, L_{b0} and L_{b6}, the operating frequency is moved to lower frequencies. In the next step, to expand the stopband, suppressing cells are required. Employing these suppressing units leads to creating some transmission nulls, thus transmission peaks will be rejected, and consequently the stopband region will be widened. One of the commonest suppression units to expand the rejection band is high-low impedance resonators with radial patches. Figures 7(a) and (b) show the configuration and the frequency response of these suppressing cells, which has two main transmission zeros at 18.75 and 25.42 GHz with corresponding attenuation levels of −28.54 and −33.27 dB, respectively. Clearly, this cell is not capable of rejecting spurious frequencies from 50 to 60 GHz. Thus, there is a need for using another suppressing resonator capable of suppressing unwanted frequencies in the above-mentioned range. Figure 7(c) illustrates a pair of polygon open-stubs creating

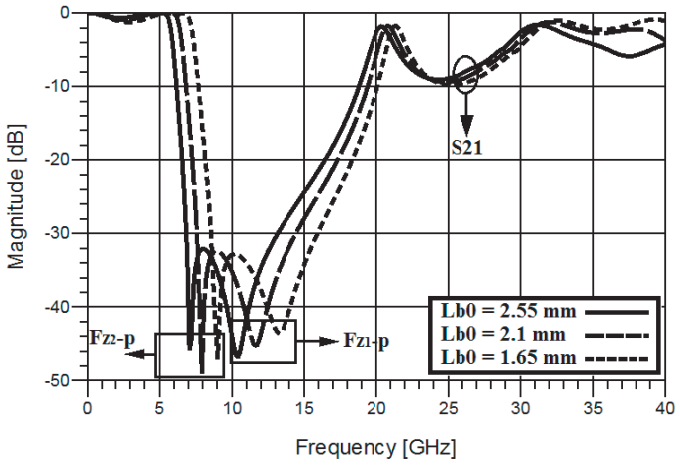

Figure 5. The behavior of the proposed polygon resonator against changing the value of L_{b0}.

an effective transmission zero at 59.62 GHz with corresponding attenuation level of −40.78 dB (see Figure 7(d)). This can help the first suppressing cell suppress spurious frequencies in a wider range. Figure 8 illustrates the combination of the introduced resonance cells leading to the final configuration of the proposed lowpass filter. As it can be seen, four main parts, i.e., polygon patches of resonators 1, T-shaped resonant cells as resonators 2, radial and polygon stubs as suppressing cells demonstrate the designed filter. Figure 9 shows the effect of adding each resonator on the frequency response, step by step. As can be seen from Figure 9(a), resonator 1 has a −3 dB cut-off frequency at 5.33 GHz and a transmission zero (T_{Z1}) at 7.708 GHz with attenuation level of −51.831 dB. Moreover, in this resonator a stopband from 6.38 GHz up to 22.39 GHz with corresponding attenuation level better than −20 dB

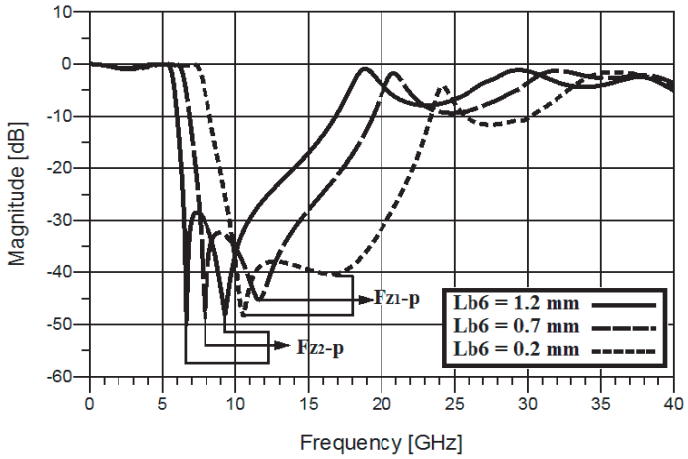

Figure 6. The behavior of the proposed polygon resonator against changing the value of L_{b6}.

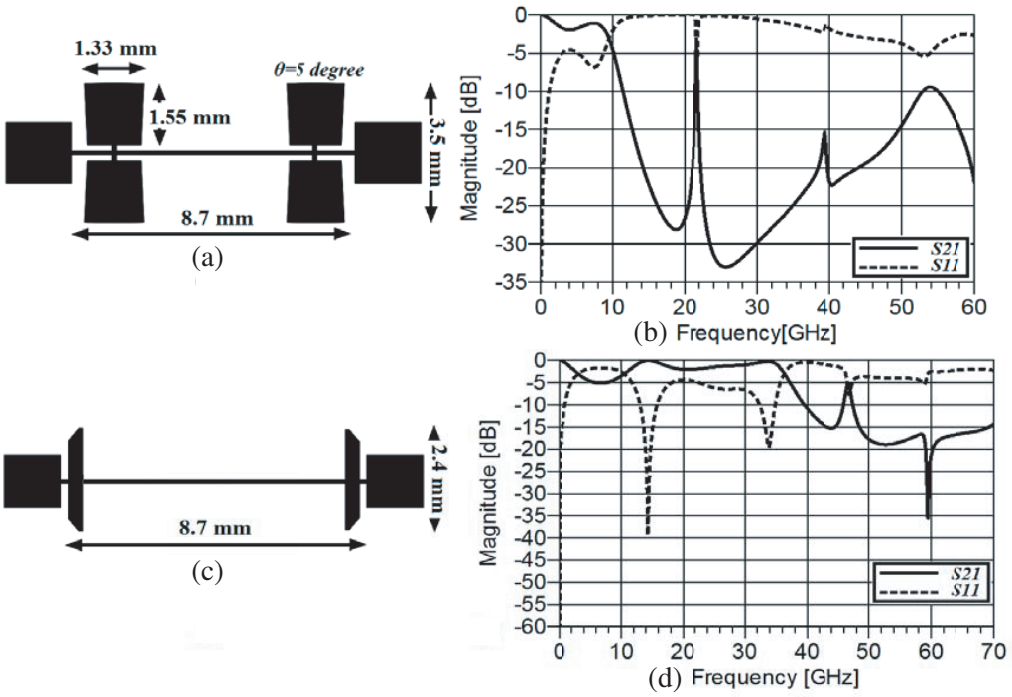

Figure 7. (a) The configuration of the first suppression units using high-low impedance resonators with radial patches. (b) Its frequency response. (c) The configuration of the second suppression units using polygon stubs. (d) Its frequency response.

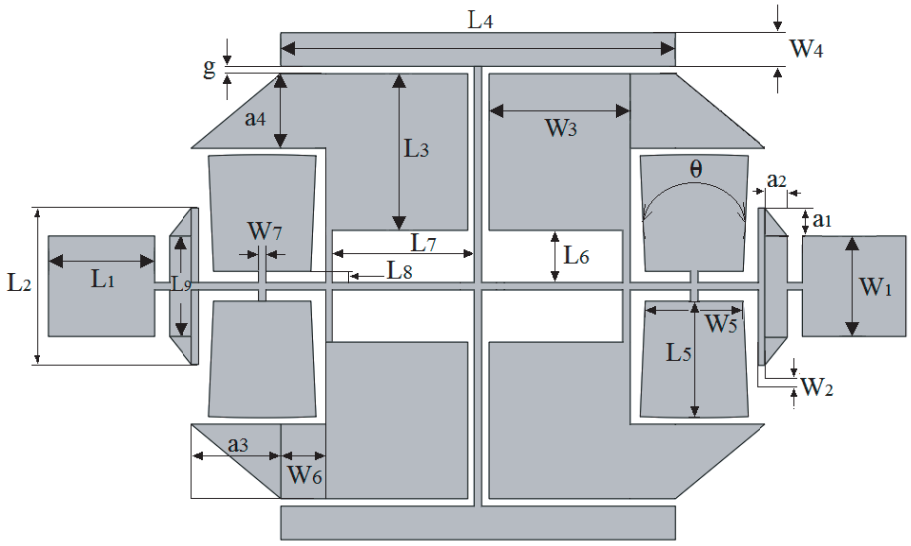

Figure 8. The configuration of the proposed lowpass filter.

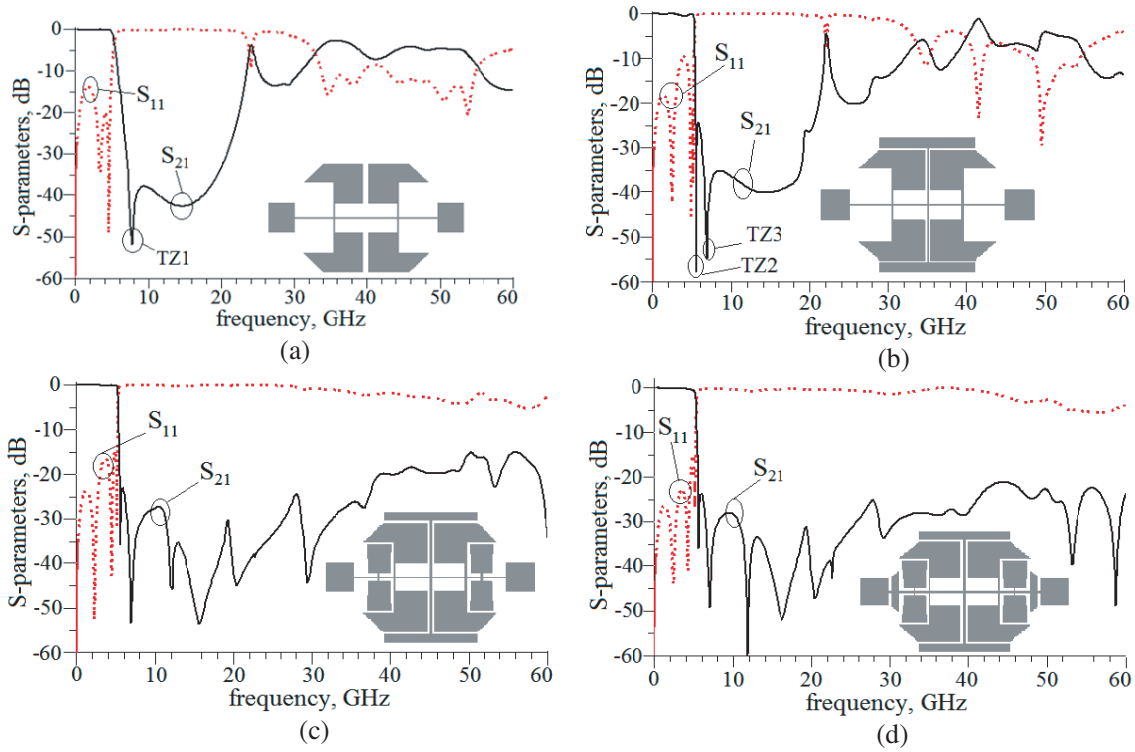

Figure 9. The frequency response of (a) resonator 1, (b) resonators 1 and 2, (c) resonators 1, 2 and the first suppressing cell, (d) resonators 1, 2, and both suppressing cells.

is obtained. However, resonator 1 does not have a sharp roll-off and wide stopband bandwidth. In order to improve the transition band, T-shaped resonators are added, as shown in Figure 9(b). The combination of resonators 1 and 2 has two transmission zeros (T_{Z2} and T_{Z3}) at 5.565 and 6.853 GHz with corresponding attenuation levels of -57.909 and -54.946 dB, respectively. In fact, by adding resonator 2 the transmission zero of resonator 1, T_{Z1}, has been shifted to the lower frequencies and T_{Z2} has been achieved. Shifting T_{Z1} to lower frequencies leads to a sharp transition band about 0.231 GHz from -3 to

-40 dB. Moreover, T-shaped resonators create a new transmission zero of T_{Z3}. However, the stopband bandwidth is not wide enough. To improve the width of the stopband with a high attenuation level, four radial stubs as the first suppressing cells can be employed, as shown in Figure 9(c). By combining resonators 1, 2 and the first suppressing cells, the stopband expands from 5.47 up to 38.75 with a suppressing level better than -20 dB. Furthermore, the insertion loss less than -0.2 dB and return loss better than -14 dB in the passband are achieved.

In order to enhance the stopband bandwidth more than $10fc$ ($fc = 5.3$ GHz) with an attenuation level of -21 dB, the second suppressing cells, i.e., two polygon stubs, are utilized. Finally, a compact LPF with -3 dB cutoff frequency of 5.3 GHz, a sharp transition band (0.2 GHz from -3 to -40 dB) and an ultrawide stopband (54.5 GHz) is designed, as shown in Figure 9(d). The dimensions of the proposed LPF are as follows (All in millimeter): $L1 = 1.6$, $L2 = 2.3$, $L3 = 2.1$, $L4 = 5.3$, $L5 = 1.5$, $L6 = 0.7$, $L7 = 1.9$, $L8 = 0.15$, $L9 = 1.55$, $A1 = 0.375$, $a2 = 0.3$, $a3 = 1.2$, $a4 = 1$, $W1 = 1.55$, $w2 = 0.1$, $w3 = 1.9$, $w4 = 0.45$, $w5 = 1.3$, $w6 = 0.6$, $w7 = 0.6$, $g = 0.1$. Finally, the equivalent LC circuit of the proposed LPF has been shown in Figure 10(a). L_1, L_2, L_3 and L_4 are equivalent inductors caused by the main transmission line. The designed T-shaped resonators are modeled by L_7 and C_{12}, where L_7 determines high impedance transmission lines of these resonators, and C_{12} shows low impedance open-circuit transmission line. Moreover, the proposed resonator with polygon patches has been modeled by L_6 and C_{11}, where L_6 accounts for high impedance transmission lines of this resonator and C_{11} models its polygon patches.

The gaps g_1, g_2, g_3 and g_4 between low impedance open-circuit lines cause coupling effects, which are modeled by C_{1g}, C_{2g}, C_{3g} and C_{4g}. Furthermore, C_1, C_2, C_3, C_4, C_5 and C_6 present the capacitance between the microstrip structure and the ground. The values of inductors and capacitors of the shown LC circuit in Figure 10(a) are [12]: $C_1 = 2.86$ fF, $C_2 = 98.5$ fF, $C_3 = 30$ fF, $C_4 = 120$ fF, $C_5 = 63.5$ fF,

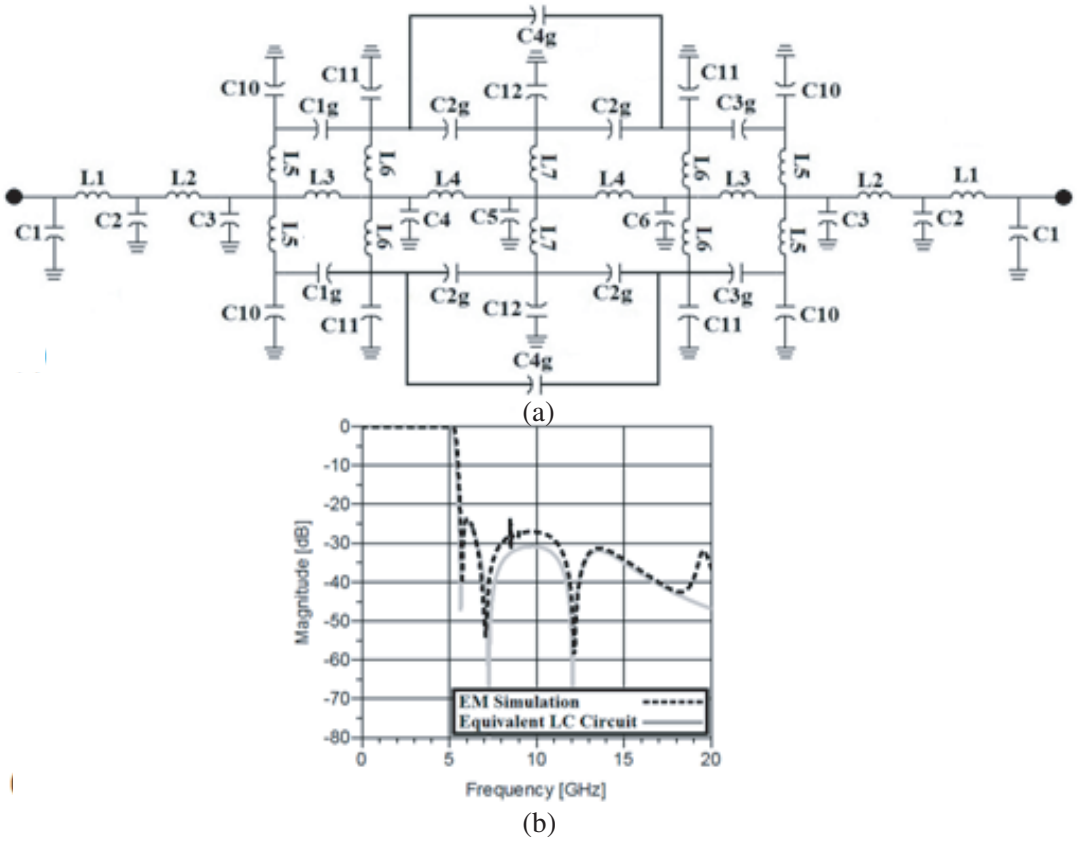

Figure 10. (a) The equivalent LC circuit of the proposed LPF. (b) The frequency response of the equivalent LC circuit.

$C_6 = 120\,\text{fF}$, $C_{10} = 85\,\text{fF}$, $C_{11} = 302\,\text{fF}$, $C_{12} = 250\,\text{fF}$, $C_{1g} = 55\,\text{fF}$, $C_{2g} = 33\,\text{fF}$, $C_{3g} = 55\,\text{fF}$, $C_{4g} = 17\,\text{fF}$, $L_1 = 0.15\,\text{nH}$, $L_2 = 0.9\,\text{nH}$, $L_3 = 0.58\,\text{nH}$, $L_4 = 1.36\,\text{nH}$, $L_5 = 0.5\,\text{nH}$, $L_6 = 0.105\,\text{nH}$, $L_7 = 2.1\,\text{nH}$. Note that one of the main resonators playing a vital role in the structure of the proposed LPF, i.e., the T-shaped shown in Figure 1(a) has been modeled by C_{12} and L_7 and the other one, i.e., the polygon resonator shown in Figure 4(a) has been modeled by C_{11} and L_6 The frequency response of the equivalent LC circuit of the proposed LPF has been shown in Figure 10(b), which is in good agreement with the EM simulation of the final circuit. As can be observed from the simulation results, the proposed filter has a $-3\,\text{dB}$ operating frequency of 5.293 GHz. In the passband region, the insertion loss is approximately zero from DC to 5.11 GHz indicating a flat response in this band. Moreover, the designed LPF has a transmission zero around the operating frequency at 5.49 GHz, which causes a desired transition band from 5.293 to 5.498 with corresponding attenuation levels of -3 and $-40\,\text{dB}$, respectively. Moreover, a suppressing level of about $-25.8\,\text{dB}$ over the shown frequency range has been obtained.

3. MEASUREMENT AND SIMULATION RESULTS

A photograph of the proposed LPF is illustrated in Figure 11(a). The proposed LPF has been designed, fabricated and tested. The implemented LPF has been constructed on a substrate with the thickness of 0.508 mm, permittivity of 3.38 and loss tangent of 0.0021. The simulated and measured frequency responses of the proposed LPF are shown in Figure 11(b). As can be seen, $-3\,\text{dB}$ cutoff frequency of the filter is located at 5.3 GHz. In the whole passband region, the insertion loss is close to $-0.2\,\text{dB}$, which shows a flat response. Moreover, in this band the return loss is better than 17 dB. As observed, close to the operating frequency two transmission zeros (TZs) at 5.511 and 5.593 GHz with attenuation levels of -43.85 and $-57.56\,\text{dB}$, respectively, exist causing a sharp roll-off rate. Thanks to these TZs, a steep transition band about 0.2 GHz from 5.3 up to 5.5 GHz with corresponding attenuation levels of -3 and $-40\,\text{dB}$, respectively, has been measured, which verifies a desired skirt performance.

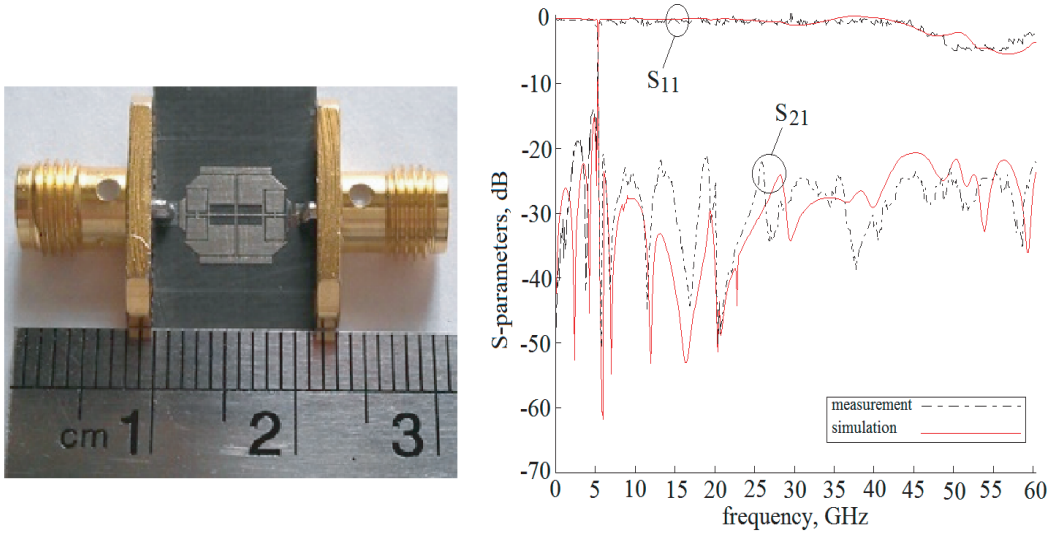

Figure 11. (a) The configuration of the proposed LPF. (b) The simulated and measured results of the proposed filter.

The stopband region suppresses spurious frequencies from 5.415 up to 60 GHz with corresponding rejection level of $-21\,\text{dB}$. Table 1 shows the performance comparison of other published works and the proposed LPF. In this table the roll-off rate is defined as:

$$\zeta = \frac{\alpha_{\max} - \alpha_{\min}}{f_s - f_c}\,(\text{dB/GHz}) \tag{6}$$

Table 1. Comparison between the performance of the proposed lowpass filter and previous works.

Ref.	Roll-Off Rate (ζ)	Relative Stopband Bandwidth (RSB)	Suppression Factor (SF)	Normalized circuit size (NCS)	Architecture Factor (AF)	Figure of merit (FOM)
[1]	30	1.25	1.5	0.080×0.080	1	8789
[2]	61.6	1.44	1	0.272×0.236	1	1386
[3]	62	1.72	3	0.310×0.240	1	4430
[4]	22	1.55	1.5	0.089×0.081	1	7095
[5]	37	1.65	1.5	0.111×0.091	1	9065
[6]	36.3	1.323	1.5	0.079×0.079	1	11543
[7]	37	1.15	2	0.280×0.076	1	3999
[8]	95	1.4	2	0.214×0.104	1	11951
[9]	130	0.933	2	0.227×0.089	2	6004
[10]	200	1.36	2	0.801×0.374	1	1815.9
This Work	**185**	**1.666**	**2.1**	**0.227×0.177**	**1**	**16181**

where $\alpha_{\max}$ is the $-40\,\text{dB}$ attenuation point and $\alpha_{\min}$ the $-3\,\text{dB}$ attenuation point; f_s is the $-40\,\text{dB}$ stopband frequency and f_c the $-3\,\text{dB}$ cutoff frequency. The relative stopband bandwidth (RSB) is given by:

$$\text{RSB} = \frac{\text{stopband bandwidth}}{\text{stopband center frequency}} \tag{7}$$

The relative stopband bandwidth (RSB) of the lowpass filter is about 166.6%. The suppression factor (SF) is based on the stopband suppression. For, example if the stopband suppression is under 21 dB, then the SF is considered as 2.1. The normalized circuit size (NCS) is given by:

$$\text{NCS} = \frac{\text{physical size (length} \times \text{width)}}{\lambda g^2} \tag{8}$$

where λ_g is the guided wavelength at 3 dB cutoff frequency. The architecture factor (AF) can be recognized as the complexity factor of the circuit, which is defined as 1 when the design is 2D and as 2 when the design is 3D. Finally, the figure-of-merit (FOM) is the overall index of the proposed filter, which is defined as:

$$\text{FOM} = \frac{\text{RSB} \times \zeta \times \text{SF}}{\text{AF} \times \text{NCS}} \tag{9}$$

4. CONCLUSION

A lowpass filter using polygon patch resonant cells, T-shaped resonators and two different suppressing cells has been designed and fabricated. Based on their equivalent LC circuits, the locations of transmission zeros of the mentioned resonators have been calculated. Moreover, good frequency performance has been obtained according to the measurement results. The proposed circuit demonstrates a sharp transition band and an ultra-wide stopband. Furthermore, this structure has low insertion loss and low return loss in the passband and also a small occupied area of $8.7 \times 6.8\,\text{mm}^2$.

REFERENCES

1. Wei, X. B., P. Wang, M. Q. Liu, and Y. Shi, "Compact wide-stopband lowpass filter using stepped impedance hairpin resonator with radial stubs," *IEE Electron. Lett.*, Vol. 47, No. 15, 862–863, Jul. 2011.

2. Wei, F., L. Chen, X.-W. Shi, Q.-L. Huang, and X.-H. Wang, "Compact lowpass filter with wide stop-band using coupled-line hairpin unit," *Electron. Lett.*, Vol. 46, No. 1, 88–90, 2010.
3. Ma, K. and K. S. Yeo, "New ultra-wide stopband low-pass filter using transformed radial stubs," *IEEE Trans. Microw. Theory. Tech.*, Vol. 59, No. 3, 604–611, Mar. 2011.
4. Cui, H., J. Wang, and G. Zhang, "Design of microstrip lowpass filter with compact size and ultra-wide stopband," *IEE Electron. Lett.*, Vol. 48, No. 14, 856–857, Jul. 2012.
5. Wang, J., H. Cui, and G. Zhang, "Design of compact microstrip lowpass filter with ultra-wide stopband," *IEE Electron. Lett.*, Vol. 48, No. 14, 854–856, Jul. 2012.
6. Wang, J., L.-J. Xu, S. Zhao, Y.-X. Guo, and W. Wu, "Compact quasi-elliptic microstrip lowpass filter with wide stopband," *IEE Electron. Lett.*, Vol. 46, No. 20, 1384–1385, 2010.
7. Luo, S., L. Zhu, and S. Sun, "Stopband-expanded low-pass filters using microstrip coupled-line hairpin units," *IEEE Microw. Wireless Compon. Lett.*, Vol. 18, No. 8, 506–508, Aug. 2008.
8. Velidi, V. K. and S. Sanyal, "Sharp roll-off lowpass filter with wide stopband using stub-loaded coupled-line hairpin unit," *IEEE Microw. Wireless Compon. Lett.*, Vol. 21, No. 6, 301–303, Jun. 2011.
9. Mandal, M. K., P. Mondal, S. Sanyal, and A. Chakrabarty, "Low insertion-loss, sharp rejection and compact microstrip lowpass filter," *IEEE Microw. Wirel. Compon. Lett.*, Vol. 16, No. 11, 600–602, 2006.
10. Gomez-Garcia, R., M. A. Sanchez-Soriano, M. Sanchez Renedo, G. Torregrosa-Penalva, and E. Bronchalo, "Extended-stopband microstrip lowpass filter using rat-race directional couplers," *Electron. Lett.*, Vol. 49, No. 4, 272–274, 2013.
11. Abdipour, A., A. Abdipour, and S. Lotfi, "A lowpass filter with sharp roll-off and high relative stopband bandwidth using asymmetric high-low impedance patches," *Radioengineering*, Vol. 24, No. 3, 712–716, 2015.
12. Hong, J.-S. and M. J. Lancaster, *Microstrip Filters for RF/Microwave Applications*, John Wiley & Sons, Inc., 2001.
13. Boutejdar, A., "Design of a very compact U-HI-LO low-pass filter using meander technique and quasi horn inductors for L-band and C-band applications," *Microwave and Optical Technology Letters*, Vol. 58, No. 12, 2897–2901, 2016.
14. Boutejdar, A., et al., "A simple transformation from lowpass to bandpass filter using a new quasi-arrow head defected ground structure resonator and gap-J-inverter," *Microwave and Optical Technology Letters*, Vol. 58, No. 4, 947–953, 2016.
15. Boutejdar, A., et al., "DGS resonators form compact filters," *Microwaves and RF*, Vol. 54, No. 3, 52–60, 2015.
16. Boutejdar, A., "Design of broad-stop band low pass filter using a novel quasi-Yagi-DGS-resonators and metal box-technique," *Microwave and Optical Technology Letters*, Vol. 56, No. 3, 523–528, 2015.